PAGEOPH, Vol. 142, No. 3/4 (1994)

0033-4553/94/040749-27$1.50 + 0.20/0

Triaxial Testing of Lopez Fault Gouge at 150 MPa Mean Effective Stress

DAVID R. SCOTT,[1,2] DAVID A. LOCKNER,[3] JAMES D. BYERLEE,[3] and CHARLES G. SAMMIS[4]

Abstract—Triaxial compression experiments were performed on samples of natural granular fault gouge from the Lopez Fault in Southern California. This material consists primarily of quartz and has a self-similar grain size distribution thought to result from natural cataclasis. The experiments were performed at a constant mean effective stress of 150 MPa, to expose the volumetric strains associated with shear failure. The failure strength is parameterized by the coefficient of internal friction μ, based on the Mohr-Coulomb failure criterion.

Samples of remoulded Lopez gouge have internal friction $\mu = 0.6 \pm 0.02$. In experiments where the ends of the sample are constrained to remain axially aligned, suppressing strain localisation, the sample compacts before failure and dilates persistently after failure. In experiments where one end of the sample is free to move laterally, the strain localises to a single oblique fault at around the point of failure; some dilation occurs but does not persist. A comparison of these experiments suggests that dilation is confined to the region of shear localisation in a sample. Overconsolidated samples have slightly larger failure strengths than normally consolidated samples, and smaller axial strains are required to cause failure. A large amount of dilation occurs after failure in heavily overconsolidated samples, suggesting that dilation is occurring throughout the sample. Undisturbed samples of Lopez gouge, cored from the outcrop, have internal friction in the range $\mu = 0.4$–0.6; the upper end of this range corresponds to the value established for remoulded Lopez gouge. Some kind of natural heterogeneity within the undisturbed samples is probably responsible for their low, variable strength. In samples of simulated gouge, with a more uniform grain size, active cataclasis during axial loading leads to large amounts of compaction. Larger axial strains are required to cause failure in simulated gouge, but the failure strength is similar to that of natural Lopez gouge.

Use of the Mohr-Coulomb failure criterion to interpret the results from this study, and other recent studies on intact rock and granular gouge, leads to values of μ that depend on the loading configuration and the intact or granular state of the sample. Conceptual models are advanced to account for these discrepancies. The consequences for strain-weakening of natural faults are also discussed.

Key words: Rock mechanics, earthquakes, friction, faulting, pore pressure, consolidation, dilatancy.

[1] Southern California Earthquake Center, University of Southern California, CA, U.S.A.

[2] Now at: Dept. of Geological Sciences, University College London, Gower St., London WC1E 6BT, U.K.

[3] United States Geological Survey, Menlo Park, CA, U.S.A.

[4] Department of Geological Sciences, University of Southern California, CA, U.S.A.

1. Introduction

Earthquakes and faults are distinctive features of crustal deformation, but basic problems about their behavior remain unsolved. The distribution of stress around major seismogenic faults, and the detailed nature of the earthquake instability, are not fully understood. As a consequence, there is at present no clear basis for predicting how the crust will deform at any time scale.

Under the circumstances, systematic experimental studies represent the best chance for stimulating the conceptual breakthroughs that are needed. Friction and failure in crustal rocks has been studied using several different experimental methods, addressing many different problems in the general area of crustal mechanics. This study was conceived to examine a material of particular interest (a natural fault gouge), using a well-established experimental method (triaxial compression) that has not previously been systematically applied to this material. While ultimately seeking to address the problems of crustal stress distribution and earthquake nucleation, this study has an exploratory character.

The choice of material, Lopez fault gouge, is motivated by recent work on its textural and mechanical properties. The provenance and composition of Lopez gouge is discussed below; it is proposed as a generic example of natural granular fault gouge. The grain size distribution in Lopez gouge has been studied in detail by SAMMIS *et al.* (1987) and SAMMIS and BIEGEL (1989), and shown to be self-similar (this distribution is also referred to as power-law or fractal). A kinematic theory for the origin of the self-similar distribution has been proposed by SAMMIS *et al.* (1987), in which grain fragmentation is controlled by the relative size of neighboring grains in the gouge. This theory is supported empirically by shearing experiments on simulated gouge (MARONE and SCHOLZ, 1989; BIEGEL *et al.*, 1989) in which the self-similar distribution develops from a uniform distribution by cataclasis during shear strain. The insight into the micromechanics of grain fragmentation in gouge provided by this theory provokes closer examination of the frictional properties of gouge.

In the chosen experimental configuration, triaxial compression, a cylindrical sample is compressed axially while confined radially by a fluid pressure medium. A particular advantage of this configuration is that precise measurements of volumetric changes can be made, by using jacketed, fluid-saturated samples with independent control of the pore pressure. This choice of experimental configuration is hardly innovative: it has been routinely used to test intact rocks up to high pressures, and soils at low pressure. There is, however, a limited amount of previous work on triaxial testing of granular materials under crustal stress conditions.

CHESTER and LOGAN (1986) present the only previous work on triaxial testing of undisturbed fault gouge, taken from the Punchbowl fault zone. They compare the mechanical properties of fault gouge, adjacent damaged rock and more distal intact rock. The experiments on gouge were not continued to high enough axial strains to produce failure (i.e., a peak in the differential stress).

ZOBACK and BYERLEE (1976a,b) measured the hydraulic properties of Ottawa sand and crushed Westerly granite during triaxial compression at confining pressures between 5 and 200 MPa. Large axial strains were required to reach failure. Before failure, substantial reduction in the pore volume produced very large reductions in the permeability, associated with grain crushing. Around and after failure, the materials dilated but a corresponding increase in permeability was not observed.

JONES (1980) measured the shear and volumetric behavior of weakly-cemented Kayenta sandstone in triaxial compression, at confining pressures between 50 and 400 MPa. Particular attention was paid to parallels with soil behavior, including dilatancy and the effects of overconsolidation.

There is, indeed, a large body of experimental and theoretical work on granular materials at lower stresses from soil mechanics. However, it is plausible that the constitutive behavior might be somewhat different at stress levels large enough to activate the process of grain fragmentation (cataclasis). For example, a study by YAMAMURO and LADE (1993) on Cambria sand (a fine lithic gravel) provides a bridge between the geotechnical and geological stress regimes. They deformed large, uniformly-prepared samples in triaxial compression and extension, at confining pressures in the range 0.25–68.9 MPa. Amongst the conclusions of this detailed study, they report a decrease in the angle of friction as the mean effective stress increases to around 8 MPa; at higher pressures the angle of friction is nearly constant.

The present study is also intended to be complementary to work on the strength and stability of gouge layers sheared between rigid blocks. Gouge layers, either in the triaxial sawcut (e.g., MARONE *et al.*, 1990) or double-direct-shear (e.g., SCOTT *et al.*, 1994) configurations, provide a miniature simulation of a natural fault zone sandwiched between intact rock walls. In mechanical terms, the direct shear configuration corresponds to plane strain, and conditions of considerable kinematic constraint. On the other hand, triaxial compression offers very little kinematic constraint but imposes well-defined conditions of stress. In the discussion section an attempt is made to compare the results from the different loading configurations.

There is a considerable body of recent work focussing on the time- and rate-dependence of friction, because of its significance for mechanical stability and hence earthquake nucleation. This study, however, explores rate-independent constitutive properties and strain-weakening mechanisms for the earthquake instability.

2. *Experimental Method*

In the suite of experiments presented here the stress conditions imposed during loading to failure were, in almost all cases, the same. The experiments started at a reference stress state of 160 MPa confining pressure and 10 MPa pore fluid pressure, giving an effective pressure of 150 MPa. During subsequent axial loading, the

pore pressure was held constant but the confining pressure was adjusted continuously (mainly reduced) to maintain a constant mean effective stress of 150 MPa. The mean effective stress is defined as

$$\bar{\sigma}' = \tfrac{1}{3}(\sigma_z + 2p_c - 3p_p). \tag{1}$$

For example, if the axial effective stress rose to 250 MPa, the radial effective stress $(p_c - p_p)$ would drop to 100 MPa. This stress path is not necessarily a good analog of natural crustal loading. It was chosen to expose the volumetric changes associated with shear failure as clearly as possible, and to allow failure to occur after the minimum amount of axial strain. In most previous studies the confining pressure was held constant, so the mean effective stress increased during axial loading. Note that the effects of varying the prescribed mean effective stress are not explored here.

Instead of varying the stress path, other aspects of the experimental conditions were isolated for scrutiny. The first experiments were performed on undisturbed gouge samples and showed very poor reproducibility. Many of the subsequent experiments used more homogeneous, remoulded gouge samples, which gave reproducible results. For comparison with previous work, a few experiments used simulated gouge samples made of sand or crushed rock. Experiments were performed to compare normally consolidated samples and samples that were overconsolidated to reduce their initial porosity. The effect of permitting or suppressing strain localisation was investigated, by performing both "fixed-end" experiments in which the sample ends were held in axial alignment, and "free-end" experiments in which the sample ends could move laterally. The order in which the experimental results are presented here is intended to provide clarity and is not chronological.

2.1 Lopez Fault Gouge

The samples of Lopez fault gouge used in this study were collected from the outcrop described by SAMMIS *et al.* (1987), in the San Gabriel Mountains of Southern California. The Lopez fault has been interpreted as a thrust associated with the San Gabriel system; it brings Mesozoic metamorphic basement up above the Pleistocene Saugus formation, a terrigenous sandstone (OAKESHOTT, 1958). The amount of vertical displacement on the Lopez fault is estimated by OAKESHOTT to be 250 m (800 feet), so the amount of slip might be 350 m.

The gouge outcrop used for sampling forms a bank to one side of a creek bed and supports very little vegetation. Although this bank is probably the toe of a large slump (about 200 m wide and high), the outcrop appears undisturbed. The gouge is easily excavated to form a fresh face a foot or two into the bank (samples were collected in the late spring, when the gouge was quite damp). The fresh face is predominantly white with some orange discoloration and infrequent green bands a few centimeters thick. The homogeneous white gouge is completely granular and has minimal cohesion; the green material is also readily deformable but is cohesive

and clay-like. The white gouge was used in all the experiments but samples of the green gouge were also collected for mineralogical analysis. Occasionally, small roots of vegetation were found in the gouge outcrop, generally following the green bands.

The mineralogy of samples from both the white gouge and the green bands was determined by X-ray diffraction by R. E. Ferrell at Louisiana State University. Analyses were performed on both a powder from the entire sample, and on the clay fraction only ($<2\ \mu$m, extracted by settling). The results are summarized in Table 1. Note that the white gouge contains less than 10% clay minerals, whereas around 40% of the green gouge is clay. The green bands could be the result of selective alteration of the white gouge, either before or after the pervasive cataclasis that formed the gouge. Alternatively, the green bands may represent relic texture from the banded gneiss found in places in the hanging wall of the fault. In either case, we are inclined to assume that the mechanical behavior of the gouge as a whole would be dominated by the properties of the white gouge because it is considerably more abundant. No mechanical testing of the green gouge was attempted.

The gouge composition reported here differs somewhat from that reported by SAMMIS *et al.* (1987). They found a chlorite content of 15–20% but no other clay minerals, and concluded on textural grounds that the formation of the chlorite predated cataclasis. We have no new information to confirm or deny this conclusion.

Even with this mineralogical information, it would be fair to state that the precise provenance and parentage of Lopez gouge is obscure. Further geological study of the fault and its wall rocks would be needed to determine the thickness of gouge present and to identify the parent rock. However, such detailed studies are probably more appropriate for faults with larger amounts of offset (e.g., CHESTER and LOGAN, 1987).

Lopez gouge does have, however, some merits recommending it for experimental study. The process of natural cataclasis has produced a granular material that is mostly quartz, has minimal cohesion and has a reasonably homogeneous and isotropic structure. More importantly, the origins of the self-similar grain size

Table 1

Mineralogical composition of Lopez gouge

Mineral	Wt. % White	Green
Quartz	85	50
Albite	7	10
Chlorite	1	22
Smectite	6	14
Others	1	4

Relative errors: $\pm 10\%$

distribution in Lopez gouge are most probably dominated by mechanical processes rather than the mineralogy of the parent rock or subsequent alteration.

2.2 Sample Preparation

Experiments were performed on both remoulded and undisturbed samples of Lopez gouge, and on simulated gouge consisting of either crushed Westerly granite or Ottawa sand.

Remoulded samples were prepared from a lump of Lopez gouge, around 100 g in mass, broken from a larger sample from the outcrop. This material still contained moisture carried from the field. The gouge was crumbled by hand, without crushing, sieving, or drying, to produce a rough powder with few particles exceeding 1 mm in diameter. The powder was poured into a cylindrical, hardened steel mould, 25.4 mm in diameter, confined by flat-ended sliding pistons at either end, and cold-pressed to around 10 MPa using a hand-operated bench press. The cohesion of the partially water-saturated sample formed was found to be sufficient, in the case of Lopez gouge, to allow it to be extruded from the mould and handled. The cylindrical sample, around 55 mm in length, was assembled with cylindrical, hardened steel end pieces and a ceramic filter disc, and jacketed with an inner jacket of transparent polyolefin heat-shrink tubing (see Figure 1).

Undisturbed gouge samples were collected directly from the outcrop by coring with a sharpened, thin-walled steel tube and a rubber mallet. The interior bore of the steel tube was enlarged behind the cutting edge to permit extrusion of the core by hand in the field. This process produced reasonably coherent cores 10–15 cm in length and around 25 mm in diameter. In the laboratory, each core was gently pressed into a cylindrical, hardened steel mould. Like the remoulded samples, the undisturbed gouge cores were cold-pressed to produce a right-cylindrical sample, and assembled with end caps, a filter disc and an inner jacket.

The process of coring, insertion into the mould and cold-pressing certainly create some disruption of the gouge material. CHESTER and LOGAN (1986) avoided this disruption by carving square prisms of gouge from a block with a diamond saw, supporting each cut face with a sheet of lead foil held in place by glue. The Punchbowl gouge they used contained about 13% clay, lending some cohesion to the material. Lopez gouge has about half this proportion of clay, and preparation of samples by sawing was not attempted. A simple improvement to our method would be the use of a split mould for the cold-pressing stage, which would eliminate disruption of the gouge during insertion into the mould.

Simulated gouge samples were prepared from Ottawa sand, a loose quartz sand with rounded grains around 800 μm. This sand was crushed to produce more angular fragments with a maximum grain size of around 200 μm. A preformed inner jacket was prepared by moulding heat-shrink tubing onto a smooth metal rod 25.4 mm in diameter. The rod was removed and one end of the jacket plugged with

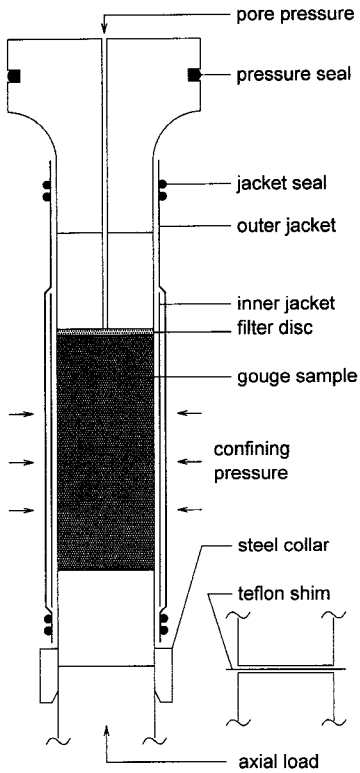

Figure 1
Schematic diagram of the triaxial sample assembly. The cylindrical gouge sample is 25.4 mm in diameter and approximately 55 mm long. Two alternate configurations are shown at the lower end. In fixed-end experiments the steel collar keeps the ends of the sample in axial alignment. In free-end experiments the teflon shim allows the lower end of the sample to move laterally, to accommodate slip in a single fault.

a steel end cap. The sand was slowly poured into the inner jacket a little at a time and tamped down, to produce a sample of reasonably uniform density. The inner sample assembly was completed with a filter disc and second steel end cap, as before.

In all cases, the inner assembly was confined in an outer jacket of either two layers of heat-shrink tubing or one layer of 3 mm polythene, and attached to a tapered, hardened steel end cap incorporating the pressure seal for the sample chamber. The plastic jacketing was sealed onto the steel end pieces using twisted steel wire (see Figure 1).

2.3 Sample Loading

The sample assembly was inserted from above into the sample chamber of the triaxial load frame and immersed in a confining pressure medium of either silicon

oil or kerosene. Independent control of the pore pressure was permitted via holes along the axis of the steel pieces at one end of the gouge sample. The ceramic filter discs prevented particles from the gouge entering the narrow-bore tubing of the pore pressure control system. The pore pressure system was evacuated and then filled with distilled water. However, the pore fluid within the natural gouge samples was natural moisture from the outcrop.

During subsequent deformation, the sample was loaded radially by the pressure of the confining fluid, and axially from below by a coaxial piston. The force on the piston was monitored by an external load cell, i.e., mounted outside the seal around the piston that contains the confining fluid. The frictional resistance of this seal was measured before loading each sample and never exceeded a few percent of the confining pressure. The confining pressure, pore pressure and axial loading rate were all separately servo-controlled by computer. Continuous (1 Hz) recordings of the following quantities were made: pore pressure, pore volume, confining pressure, axial load, and axial displacement.

Normal consolidation

The term "normal consolidation" in soil mechanics implies that the sample has not experienced a mean effective stress larger than the present mean effective stress. For example, a loose granular material that is densified by applying a monotonically increasing mean effective stress will be normally consolidated.

To create a normally consolidated sample, before the application of any axial load, the confining pressure around the sample was steadily increased to 160 MPa. Some of this load is transferred onto the pore fluid, and after the pore pressure reached 10 MPa, pore fluid was steadily pumped out of the sample to hold the pore pressure at 10 MPa. Hence the mean effective pressure was steadily increased to 150 MPa to create a normally consolidated sample under isotropic stress conditions corresponding to around 10 km depth of burial in the crust (with hydrostatic pore pressure).

Measurements on some samples determined that, during this isotropic loading, the porosity of the Lopez gouge was reduced from around 24% at room conditions (after cold-pressing) to $12 \pm 1\%$ at 150 MPa effective pressure. In subsequent calculations involving the pore volume, a porosity of 12% was assumed for all the Lopez gouge samples following isotropic loading.

Loading to failure at constant mean effective stress

The axial strain rate for most of the experiments was set at $10^{-5}\ s^{-1}$. This rate was determined empirically, to ensure that drained conditions (i.e., uniform pore

However, by holding the mean effective stress constant, the sample remains normally consolidated at all times but fails significantly sooner, typically at an axial strain of around -0.1.

Overconsolidation

A number of experiments were performed on overconsolidated samples, a term implying that the sample has a lower porosity than a normally consolidated sample. Overconsolidation can be produced by subjecting a sample to a higher mean effective pressure than that at which it is subsequently loaded to failure. These samples were prepared by first increasing the confining pressure, applying an isotropic load of up to 500 MPa. To further reduce the porosity, an axial load was also applied, but only up to around 80% of that needed to cause failure. The axial load was then removed and the confining pressure reduced to 160 MPa (150 MPa effective) for subsequent loading to failure. At this point the porosity of the overconsolidated samples was reduced to between 6.3% and 10.5%, as compared to the 12% porosity of normally consolidated samples. Inspection of a sample that was removed from the pressure vessel after overconsolidation confirmed that the sample retained its right-cylindrical shape during the application of the axial load at the elevated confining pressure.

2.4 Data Processing

The load cell records the total axial force applied to the sample. To convert this measurement to axial stress, the cross-sectional area of the sample must be known. In an intact sample of low porosity this area is well approximated by that of a circle, 25.4 mm in diameter, at least until the sample breaks. A granular sample shows a significant amount of volumetric strain during loading, and also requires substantially more axial strain to reach failure than an intact sample. The cross-sectional area of a granular sample therefore changes by a significant amount, and a corresponding correction to the axial force must be made to produce an accurate estimate of the axial stress.

The intended conditions of constant mean effective stress were not exactly maintained in these experiments, because of the uncertainty in the sample cross section and hence the true value of axial stress. For simplicity, the uncorrected axial stress (assuming a constant cross-sectional area) was used in the algorithm that varied the confining pressure to control the mean effective stress. This simplification resulted in a variation of mean effective stress of no more than 20 MPa above or below 150 MPa.

Uniform strain correction

The primary correction made to the axial stress assumes that strain is uniform throughout the sample, i.e., that the sample retains its right-cylindrical shape. This appears to be a good assumption up to the point of failure. After failure, the

assumption is clearly not correct if the strain localises to a single fault. The analytic form used to correct the cross-sectional area of the sample is derived in the Appendix.

Correction for fault slip

When localisation of strain to a "fault" was observed in a sample, after removal from the pressure vessel, a correction can be attempted for slip on the fault after the point of failure. This point may be estimated from the trends of stress and strain, or determined *a posteriori* by inspecting the sample after the experiment. A correction to the axial stress, based on the area of overlap between offset cylinders, can then be made. This derivation is also presented in the Appendix.

3. Experimental Results

A total of 19 experiments are presented in this study. A summary of the experimental conditions and results is presented in Table 2. Almost all the experiments presented are duplicated.

3.1 A Fixed-end Experiment

To illustrate the data processing method and general features of the results, Figure 2 shows data from a sample of remoulded Lopez gouge, normally consolidated and loaded to failure with its ends constrained to remain in axial alignment. This constraint was achieved by using a steel collar to link the lower steel end cap of the sample and the loading piston (see Figure 1).

The upper plot in Figure 2 shows the uncorrected axial stress and radial confining pressure as functions of the axial strain. A constant mean effective pressure is maintained by reducing the confining pressure as the axial load increases.

The lower plot in Figure 2 displays the volumetric and radial components of strain, as functions of the axial strain. The volumetric strain is calculated directly from the changes in pore fluid volume required to maintain a constant pore pressure. The initial part of the profile of volumetric strain against axial strain shows that the application of shear stress, at constant mean stress, produces additional consolidation. The profile then shows a minimum around the point of failure, followed by steady dilation for the remainder of the test.

The radial strain is calculated from the axial and volumetric strain by assuming that the volume of the solid material remains constant (elastic volume changes are minimal when the mean stress is constant), and that the strain is uniform. The radial strain is monotonically increasing, implying that the sample continuously expands radially as it is compressed axially. The rate of increase is slightly slower

Table 2

Experimental conditions and results

Expt.	Material	Initial Porosity	End Condition	Failure State			Notes
				tan ϕ	$-\epsilon_z$	$-\epsilon_v$	
001	Undisturbed Lopez	0.120	Fixed	>0.545	>0.141	0.025	(a)
002	Undisturbed Lopez	0.120	Fixed	0.605	0.136	0.012	(b)
003	Undisturbed Lopez	0.120	Fixed	0.465	0.087	0.015	
004	Undisturbed Lopez	0.120	Free	0.540	>0.071	>0.004	(c)
006a	Undisturbed Lopez	0.120	Free	0.495	0.085	0.017	
008	Undisturbed Lopez		Free	0.417	0.088	0.003	(d)
053b	Undisturbed Lopez	0.120	Free	0.499	0.087	0.020	
035	Remoulded Lopez	0.120	Fixed	0.593	0.144	0.022	
052	Remoulded Lopez	0.120	Fixed	0.574	0.144	0.017	
030	Remoulded Lopez	0.120	Free	0.620	0.100	0.016	
032	Remoulded Lopez	0.120	Free	0.605	0.117	0.024	
051b	Remoulded Lopez	0.120	Free	0.593	0.146	0.020	
034b	Remoulded Lopez	0.105	Free	0.654	0.112	0.029	(e)
036c	Remoulded Lopez	0.076	Free	0.629	0.027	0.041	(e)
055c	Remoulded Lopez	0.085	Free	0.681	0.048	0.035	(e)
056bc	Remoulded Lopez	0.063	Free	0.674	0.026	0.051	(e)
054bc	Ottawa sand	0.219	Free	0.623	0.229	0.087	
057b	Ottawa sand		Free	0.648	0.266	0.081	(f)
031	Crushed Westerly		Free	0.595	0.175	0.053	

"Initial Porosity" is at $p_c = 160$ MPa, $p_p = 10$ MPa. A uniform value of 12% is assumed for all the normally-consolidated Lopez gouge samples.

Notes:

(a) Constant confining pressure ($p_c = 160$ MPa, $p_p = 10$ MPa). Sample did not fail (tan ϕ still climbing slowly at end of experiment).

(b) Axial strain rate $= 3.5 \times 10^{-6}\ s^{-1}$.

(c) Strains to failure are lower bounds, due to procedural error.

(d) Axial strain rate $= 10^{-6}\ s^{-1}$.

(e) Overconsolidated: ϵ_v is relative to normally consolidated state.

(f) Heterogeneous mixture of coarse and fine sand.

initially, while the sample volume is decreasing. The radial strain calculated in this way is then used to correct the axial stress (see Appendix).

It is useful to represent the state of stress by defining an instantaneous angle of friction ϕ, using the following expression for $\sin \phi$:

$$\sin \phi = \frac{(\sigma_z - p_c)}{(\sigma_z + p_c - 2p_p)}. \tag{2}$$

This expression is based on the Mohr-Coulomb failure criterion for plastic materials. The point of failure coincides, by definition, with the peak value of ϕ. The corresponding peak value of $\tan \phi$ is equal to the conventional coefficient of

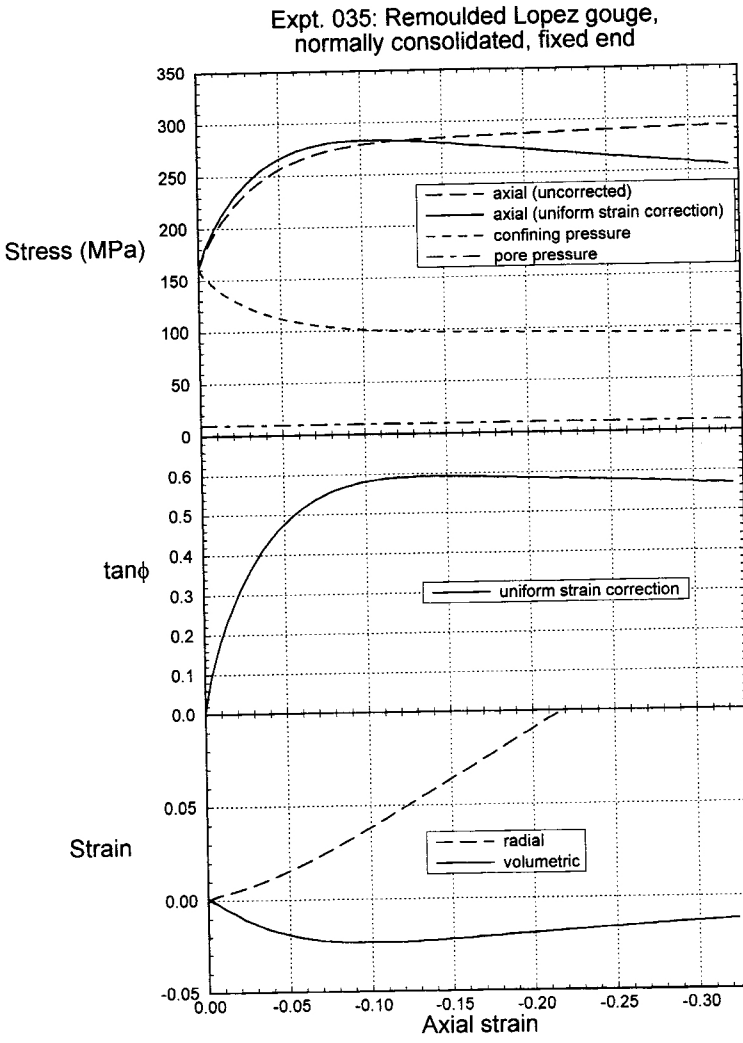

Figure 2

Results from an individual experiment using the fixed-end configuration. The sample is normally consolidated, remoulded Lopez gouge. In all the plots the horizontal coordinate is the logarithmic axial strain, relative to the sample length after hydrostatic loading to $p_c = 150$ MPa, $p_p = 10$ MPa. The upper plot shows the measured axial stress, confining pressure and pore pressure, and the corrected axial stress calculated by assuming uniform strain (see Appendix). In the middle plot the state of stress (calculated using the corrected axial stress) is parameterized by $\tan \phi$, where ϕ is the instantaneous angle of friction. The lower plot shows the measured volumetric logarithmic strain, again relative to the sample volume after hydrostatic loading. The radial strain is also shown, calculated by assuming uniform strain in the sample. The peak value of $\tan \phi$ is 0.593, at an axial strain ϵ_z of -0.144 and a volumetric strain ϵ_v of -0.022.

internal friction μ, a material property that parameterizes the failure strength. The middle plot in Figure 2 shows the quantity $\tan \phi$ as a function of axial strain.

After removal from the sample chamber and the outer jacket, the sample could be inspected while still supported by the transparent inner jacket. In this experiment the sample was shortened by 15 mm, corresponding to an axial strain of -0.33, and had assumed a barrel shape. This nonuniform distribution of sample thickening means that the "uniform strain correction" is not accurate in correcting the axial stress at large strains. The sample had remained nearly axially symmetric; the trace of one or two incipient shear planes could be seen but had not developed large displacements.

3.2 A Free-end Experiment

The experiment described above, using the steel collar, was designed to suppress shear localisation. This can be contrasted with experiments in which the lower end of the sample was permitted to move laterally, by inserting a teflon shim between the steel end cap of the sample and the loading piston (see Figure 1). The teflon shim was also coated with molybdenum grease to provide the minimum amount of frictional resistance to lateral motion. This method of assembly permits shear localisation in the sample as it deforms. Specifically, the strain localises to a single oblique shear plane at approximately 30° to the axis. Displacement on this plane moves one end of the sample laterally with respect to the other; hence the need for the teflon shim.

Figure 3 illustrates the results of an experiment using remoulded Lopez gouge, normally consolidated and loaded through failure with a 'free' end condition. The axial stress has been corrected in two ways. First, the uniform strain correction is applied to the entire stress history, and the parameter $\tan \phi$ is calculated using the corrected axial stress. The peak value of $\tan \phi$ is identified, and assumed to coincide with strain localisation to a fault. The fault slip correction is then applied to the axial stress assuming that after localisation, all sample shortening is accommodated by fault slip. This correction is then carried through to $\tan \phi$. All of these steps are illustrated in Figure 3. The results show that the fault slip correction produces a fairly constant value of $\tan \phi$ after the assumed commencement of fault slip.

In all samples with a free end condition, fault slip was very apparent in the final shape of the sample. In this experiment the sample was shortened by 10 mm, corresponding to an axial strain of -0.18; with further shortening the free end of the sample would make contact with the wall of the sample chamber. In one case (Expt. 053), a grid of lines was drawn on the moulded sample before jacketing. This grid was broken by fault slip during deformation of this sample, and a reasonably accurate estimate of the amount of fault slip could be made. In this case the fault consisted of a zone a millimeter or two across; the amount of displacement across this zone was consistent with shear localisation at the peak in $\tan \phi$, as assumed in making the fault slip correction to the axial stress.

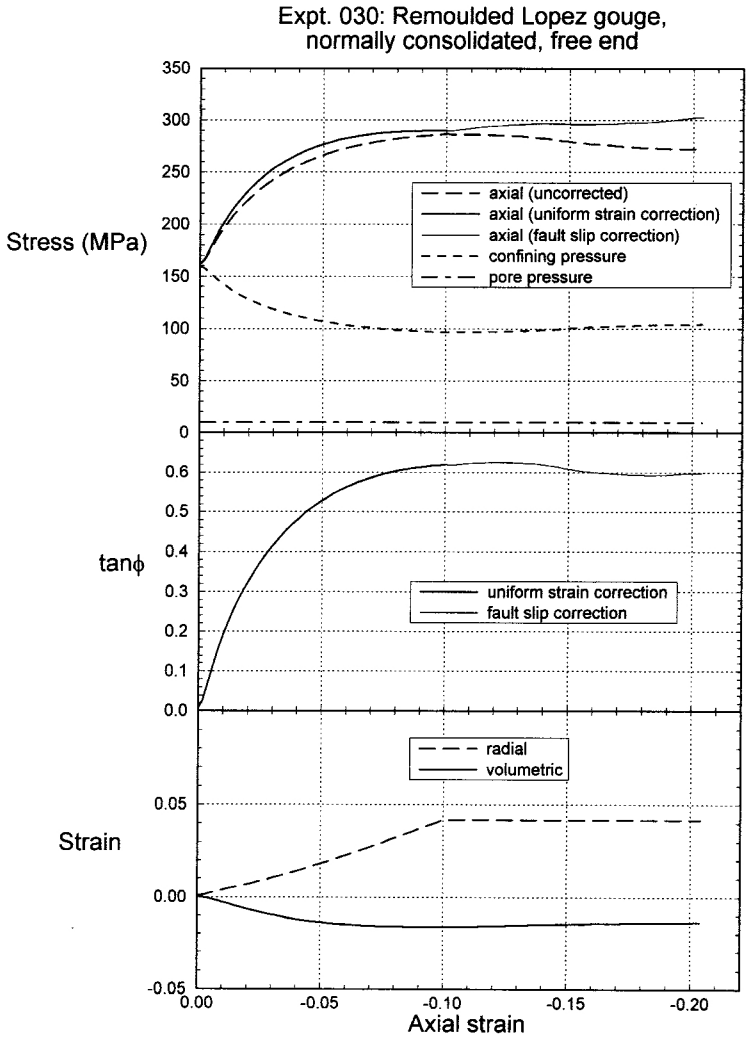

Figure 3

Results from an individual experiment using the free-end configuration. The sample is normally consolidated, remoulded Lopez gouge. The layout is in most respects the same as in Figure 2. As in Figure 2, a corrected axial stress is shown in the upper plot, calculated by assuming uniform strain. In this experiment, the free-end configuration permitted the strain to localise to a single discrete fault at some point during the loading. It is assumed that this point coincides with the peak in $\tan \phi$, calculated using the axial stress after correcting for uniform strain. After this point, the axial stress corrected for fault slip (see Appendix) is shown in the upper plot as a finer line, and the corresponding values of $\tan \phi$ are shown in the middle plot. The radial strain is assumed to remain constant following faulting. The peak value of $\tan \phi$ (after the uniform strain correction but before the fault slip correction) is 0.620, at an axial strain ϵ_z of -0.100 and a volumetric strain ϵ_v of -0.016.

3.3 Shear Localisation and Dilation

Figure 4 exhibits corrected stress and strain measurements from several experiments using remoulded, normally consolidated gouge with either "fixed"- or "free"-end conditions (i.e., experiments using the steel collar or teflon shim, respectively). Note that the peak value of $\tan \phi$ is similar in all cases, in the range of 0.6 ± 0.02. Also, the volumetric strain is similar up to the maximum in $\tan \phi$. This suggests that the nature of the end constraint only becomes significant after the point of failure.

After failure, the stress curve is less reliable because of the corrections made to the axial stress. However, the volumetric strain curves betray a subtle difference between the fixed-end and free-end experiments. As described above, the fixed-end

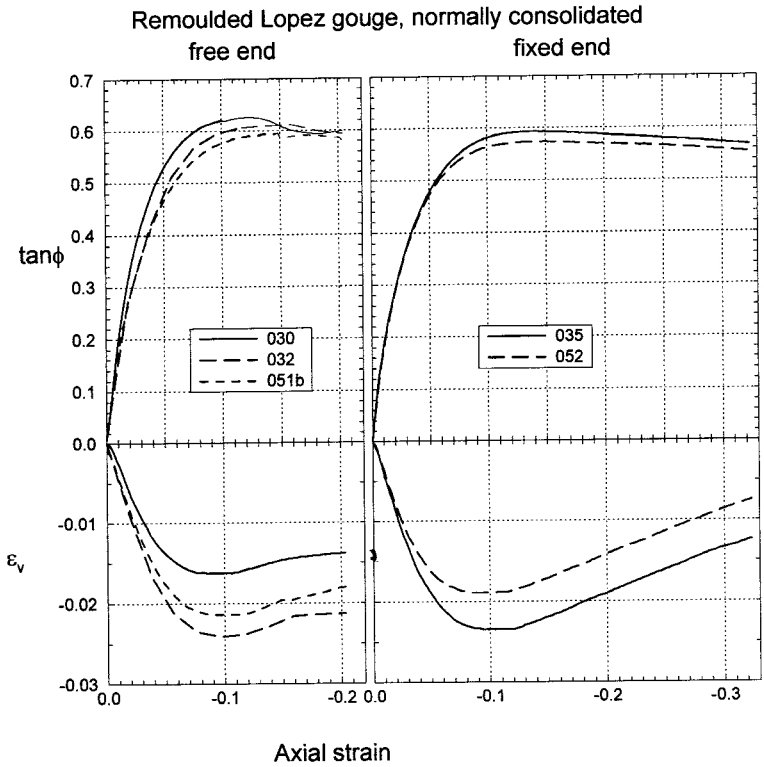

Figure 4

Summary of results from experiments using the free- and fixed-end configurations. All the samples are normally consolidated, remoulded Lopez gouge. The left-hand plots show results from three free-end experiments; the right-hand plots show results from two fixed-end experiments. The upper plots show the parameter $\tan \phi$, calculated using the uniform strain correction and, for the free-end experiments, the fault slip correction. The line width is reduced when the fault slip correction is applied. The lower plots show the volumetric strain.

samples show steady dilation after failure. The free-end samples also dilate after failure, but the rate of dilation diminishes after some further strain. This suggests that the dilation is confined to the single shear plane, along which the local porosity climbs to a stable value after a displacement of a few millimeters. In the fixed-end tests, the constraint on the strain prevents any single plane from developing very much displacement. New shear planes are continually formed, each contributing some additional dilation (apparently irreversible) to the overall volumetric strain of the sample.

It is worth noting that the use of constant mean stress in these experiments aids in identifying these subtle volumetric effects, which might otherwise be masked by larger volumetric strains associated with changes in the mean stress.

3.4 Overconsolidaton

Figure 5 shows a number of experiments performed with remoulded Lopez gouge samples that were overconsolidated, without failing, before loading to failure. Results for a single normally consolidated sample, from Figure 4, are shown for comparison. All the experiments shown used the free-end assembly. A measure of the extent of overconsolidation is the porosity under isotropic stress before the final loading to failure. In Figure 5, this is shown as an offset in the volumetric strain at zero axial strain. The extent of overconsolidation was varied by changing the amount of isotropic and shear load applied; in the extreme case (Expt. 056bc) the sample was preloaded to $p_c = 500$ MPa and $\sigma_z = 1300$ MPa.

The overconsolidated samples generally show a slightly larger failure strength and a significantly smaller strain to failure, when compared with normally consolidated samples. Most of the overconsolidated samples also show significant strain-weakening after the peak in strength. This result should be treated with caution, because all these samples showed definite faults and the fault slip correction has been applied. This correction depends strongly on the precise point at which the fault forms, which is unfortunately rather uncertain. In Figure 5, the fault is assumed to form at the peak in strength (as in Figure 3).

The volumetric behavior is again of particular interest. The most heavily overconsolidated samples show no volume strain at the very start of loading, followed by substantial dilation that commences before the peak strength is reached and continues for some time after the peak in strength. This dilation might be attributed to the formation of a fault, as in the above discussion of volume strain in the fixed- and free-end experiments on normally consolidated gouge. However, the magnitude of the dilation is an order of magnitude larger than that seen in the normally consolidated samples. It seems unlikely that a narrow fault zone, representing a very small proportion of the volume of the sample, would dilate enough to produce the observed average volume strain of around 2%. It therefore seems more probable that the dilation is distributed throughout the sample, even though the shear strain is confined to a fault plane.

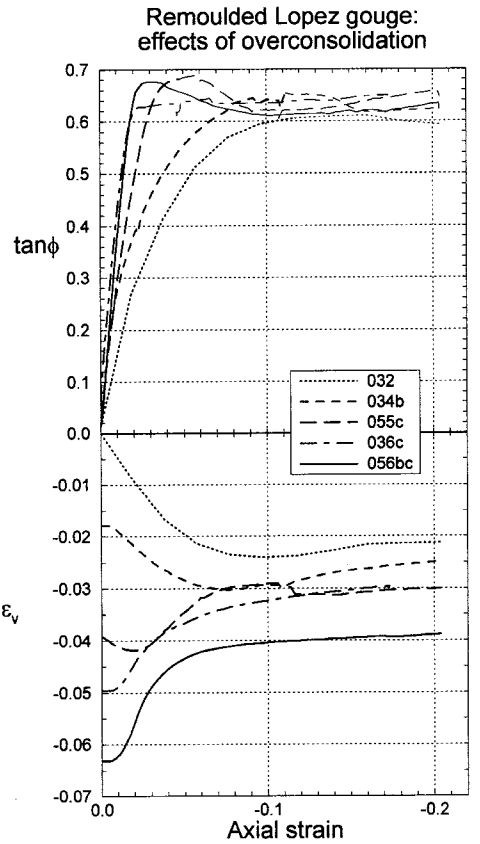

Figure 5

Summary of results from experiments with overconsolidated samples, using the free-end configuration. All the samples are remoulded Lopez gouge. The upper plot shows the parameter tan ϕ calculated using the uniform strain correction and the fault slip correction. The line width is reduced when the fault slip correction is applied. The lower plots show the volumetric strain. For comparison, results from a single normally consolidated sample are shown (Expt. 032).

Referring to the latter stages of the experiments shown in Figure 5, the final volume strain (relative to normal consolidation to $p_c = 160$ MPa, $p_p = 10$ MPa) in all the experiments reveals some convergence towards a value in the range of -0.02 to -0.04. This may represent a state favored by the bulk of the sample at or after failure, at this particular mean effective stress, regardless of the initial state of the sample.

3.5 Undisturbed Lopez Gouge and Simulated Gouge

Figures 4 and 5 show the results of all the experiments performed on remoulded Lopez gouge. A comparative discussion of the remaining experiments can be made

with reference to Table 2. The remaining experiments fall into two groups: undisturbed Lopez gouge, and simulated gouge consisting of either Ottawa sand or crushed Westerly granite.

Undisturbed Lopez gouge

Most of these experiments were performed before those with remoulded samples. The values of tan ϕ at failure are much more variable than those subsequently determined for remoulded gouge, ranging between 0.42 and 0.60. The upper end of this range corresponds to the value established for remoulded gouge. Although the initial porosities of the undisturbed and remoulded samples were quite similar, the axial strain at failure was generally smaller for the undisturbed samples.

The present data do not permit any precise statements regarding the mechanisms responsible for the low, variable strength of the undisturbed samples. Photomicrographs of thin sections of both undisturbed and remoulded samples, after deformation, were examined for obvious differences. One or two undisturbed samples show internal heterogeneity in the distribution of larger grains, but these do not correlate with the most anomalously weak samples.

The experimental results indicate that the undisturbed samples preserve some kind of natural heterogeneity that can significantly reduce their strength, as compared with the uniform value obtained for remoulded samples. This heterogeneity survives a sample preparation procedure that causes some disruption of the material.

These results open several avenues for speculation:

1. A less disruptive sample preparation procedure might produce even lower and more variable strength.

2. The effect of heterogeneity on sample strength might have some dependence on the sample size. For example, significantly larger samples with larger-scale heterogeneity might be weaker still.

3. The kinematic model for the development of a self-similar grain size distribution proposed by SAMMIS *et al.* (1987) suggests that the grain fragmentation should spontaneously produce a spatially homogeneous distribution of grains of all sizes. In reality, the process of fragmentation would be partially stochastic, perhaps allowing the development of local concentrations of large or small grains. Such configurational heterogeneity would be destroyed by the process of remoulding. Arguably, there is no reason to expect the material to be strengthened by configurational heterogeneity, so the only likely mechanical effect would be weakening.

Simulated gouge

These experiments provide some continuity with previous work (ZOBACK and BYERLEE, 1976a,b; JONES 1980), in which conditions of constant confining pressure were applied and, as a consequence, very large axial strains were required to reach failure. The results in Table 2 show that the Ottawa and Westerly samples used here

required significantly larger axial strains to reach failure than the Lopez gouge samples. The volumetric strains at failure were also a factor of two or more larger for the simulated gouge than the natural gouge. The failure strengths appear to be larger for the simulated gouge; however, confidence in the values for $\tan \phi$ is reduced because of the smaller number of experiments and the large corrections to the axial stress arising from the large strains.

Further insight is gained from measurements of the grain size distribution of the selected Lopez and Ottawa samples before and after deformation. These measurements were made by conventional sieving and settling techniques. The Lopez samples display the self-similar distribution reported by SAMMIS *et al.* (1987) and SAMMIS and BIEGEL (1989), with a large range of grain sizes and a large proportion of small grains. The distribution is essentially unmodified by the relatively small amounts of shear strain applied during these experiments. The undeformed Ottawa sand has a narrow range of grain sizes, around 200 μm. After deformation, the distribution broadens as more small grains are produced by cataclasis. The amounts of shear strain applied are too small to produce the expected self-similar distribution, but the trend is consistent with the expectation.

The differences in mechanical behavior between natural and simulated gouge can be attributed to the differences in grain size distribution. The natural Lopez gouge has a porosity of around 12% after isotropic loading; the changes in porosity during deformation are quite small. Relatively little compaction is needed to reach the state of failure, and consequently the axial strain to failure is relatively small. The simulated gouge has a porosity in excess of 20% after isotropic loading; about half this porosity is lost by inelastic compaction before failure. (In fact, the porosities of the natural and simulated gouge at failure are quite similar.) The process of inelastic compaction involves a large amount of cataclasis, as evidenced by the modification in grain size distribution. Failure is delayed while these large volumetric strains develop.

4. *Discussion*

The strategy adopted in this study, of performing experiments at a constant mean effective stress, has produced a number of novel qualitative results. In particular, the volumetric behavior associated with shear failure has been explored, and a comparison between remoulded and undisturbed natural gouge, and simulated gouge, has been made. These results are discussed in the preceding section.

This study alone does not, however, offer enough data to support a detailed quantitative model of the mechanical behavior of gouge. Instead, the following discussion attempts to explore the relevance of the main quantitative results of this study to the interpretation of other experimental results, and to the behavior of natural fault zones.

4.1 The Strength of Intact Rock and Fault Gouge

In this section, comparisons are made between the results presented here and complementary results from two other studies: SCOTT *et al.* (1994), and LOCKNER and BYERLEE (1993). If the results from all three studies are interpreted using standard plasticity with a Mohr-Coulomb failure criterion, they predict values of the internal friction μ that vary substantially as a function of the loading geometry and the state of the material (intact or granular). These studies appear to frame a genuine paradox, without offering enough data to constrain its solution. The following discussion is necessarily speculative but attempts to identify some of the relevent factors.

This discussion is built in part on the analysis of the behavior of gouge in a fault zone presented by BYERLEE and SAVAGE (1992), who show how a Coulomb material confined to a fault zone evolves to a steady state in which the apparent friction of the fault zone is $\sin \phi$, where $\tan \phi$ is the internal friction of the gouge. The existence of this state had been suggested previously (HANSEN, 1961; MANDL *et al.*, 1977; HOBBS *et al.*, 1990; MARONE *et al.*, 1992), for both theoretical and experimental reasons. SCOTT *et al.* (1994) extended the plasticity analysis to include the effects of thinning and densification of the fault zone.

To provide a point of reference, the results shown in Figure 4 indicate that the coefficient of internal friction (the peak value of $\tan \phi$, assuming no cohesion) for normally consolidated, remoulded gouge in triaxial compression is within the range $\mu = 0.6 \pm 0.02$. The gouge is water-saturated and loaded in triaxial compression at a mean effective stress of 150 MPa. In Figure 5, overconsolidated gouge shows slightly greater strength and some strain-weakening.

SCOTT *et al.* (1994) presented data from double-direct-shear experiments on granular gouge. The gouge was room-dry and loaded in plane strain at a mean stress of 25 MPa. The measurements of apparent friction required correction because the orientation of the principal stresses in a sheared layer is not directly measured. Corrections were also made for the effects of extrusion and densification of the gouge. The data from a number of experiments on simulated and natural gouge (in plane strain) were then found to be consistent with a value of internal friction in the range $\mu = 0.85 \pm 5\%$, again assuming no cohesion.

LOCKNER and BYERLEE (1993) presented data on the failure conditions of intact granite in triaxial compression, and compared them with data on the frictional resistance of sawcut "faults" in granite under the same loading conditions. The intact samples fail by the formation of an oblique fracture; the intact samples then resemble, in principle, the sawcut samples. However, the intact samples were systematically stronger than the sawcut samples over a range of confining pressures. These results were reconciled by proposing that the strain in the sawcut samples is accommodated in a "fault zone" of finite width, containing granular material that deforms by plasticity. Again, the characteristic of a finite plastic fault zone is that the ratio of the shear and normal stresses (aligned with the

fault plane) does not exceed an apparent coefficient of friction equal to $\sin \phi$, where $\tan \phi$ is the internal friction of the fault gouge. LOCKNER and BYERLEE (1993) implicitly argue that, in their experiments on intact samples, the principal stresses remain aligned with the axes of the sample, at least up to the point of failure by fracturing. Thus, these experiments directly measure $\tan \phi$. Good agreement between the intact and sawcut experiments is found if it is assumed that they measure $\tan \phi$ and $\sin \phi$, respectively. At normal stresses below 200 MPa, the apparent friction $\sin \phi$ has a roughly constant value of 0.85 (BYERLEE, 1978), corresponding to an internal friction $\mu = 1.6$.

The expectation that the internal friction should be constant is not supported by the observations summarized above. It is not, for example, always possible to predict the failure conditions for experiments performed in one geometry from those performed in another geometry.

One solution to this problem is to propose that the material property (internal friction) actually depends on specific details of the loading configuration. For example, the internal friction of gouge in a sheared layer appears significantly greater than gouge in triaxial compression. The Mohr-Coulomb failure criterion, used to define ϕ and hence μ through Equation (2), considers only the maximum and minimum principal effective stresses. It has been recognized for some time in soil and rock mechanics (e.g., GREEN and BISHOP, 1966; MOGI, 1967; AMADEI and ROBINSON, 1986; MANDL, 1988; TAKAHASHI and KOIDE, 1989) that the intermediate principal effective stress also affects the failure conditions. In the triaxial compression experimental configuration, the two smaller principal effective stresses are both equal to $p_c - p_p$. If the intermediate stress is increased (e.g., by using a "true triaxial" experimental configuration) the Mohr-Coulomb internal friction increases. (The internal friction may decrease somewhat as the intermediate and maximum principal effective stresses become equal, i.e., in triaxial extension.) For a sheared layer in plane strain, the intermediate principal effective stress is approximately mid-way between the maximum and minimum values, thus the measured internal friction of gouge should be greater than in triaxial compression.

The contrast between $\mu = 0.6$ for triaxial compression and $\mu = 0.85$ (or more) for plane strain is nonetheless unusually large, and it is possible that some other difference between the two sets of experiments may contribute to this contrast. For example, the mean stress in the double-direct-shear experiments of SCOTT *et al.* (1994) was 25 MPa, considerably smaller than the mean effective stress of 150 MPa used here. Also, the double-direct-shear experiments were performed on dry gouge, which might be somewhat stronger than water-saturated gouge. However, an exploratory experiment was performed on dry gouge in triaxial compression and produced a similar failure strength to the wet gouge.

BYERLEE and SAVAGE (1992) emphasize the role of the boundary conditions imposed by the intact walls of the fault zone in controlling the strain within fault

gouge. The imposed strains in turn control the orientation of the stress tensor and hence the apparent friction. In contrast to the low-compliance boundary conditions applied to gouge between effectively rigid fault walls, the boundary conditions applied in triaxial compression are highly compliant. The principal stresses are therefore expected to remain aligned with the sample, at least in the fixed-end experiments. Even in the free-end experiments, when a localised shear zone develops, there remains a relatively minor contrast in strength and rigidity between the gouge inside and outside the shear zone. In particular, the gouge outside the layer should not have sufficient rigidity to impose a zero-strain boundary condition on, or to rotate the principal stresses within, the shear zone. In the absence of some kind of "apparent friction" effect based on stress rotation, the low internal friction of the gouge would have to be accepted as a material property. At the micro-mechanical scale, the individual grains may exploit the high-compliance boundary conditions by local lateral movements, resulting in a reduced macroscopic internal friction (at constant intergranular friction).

Alternatively, the final state of the free-end experiments (i.e., with a narrow shear zone) could be interpreted in terms of a local bifurcation in the orientation of stresses. Within the zone, the material is in a state of failure, with the principal stresses rotated to 45° to the shear zone (or about 15° to the sample axis). The state of stress outside the shear zone only matches the normal and shear stress at the planar boundary with the zone. The material outside the zone can therefore lie below the failure surface, retaining sufficient elastic strength to provide a low-compliance boundary condition for the shear zone. The measurements would then be interpreted by relabelling the "tan ϕ" axis in, for example, Figure 3 as "sin ϕ." The implied internal friction would then be $\mu = 0.75$, which would be easier to reconcile with the results from sheared layers. The problem with this idea is that the local bifurcation in stress must start early in the deformation, before significant localised strain has accumulated; otherwise, a peak strength of $\tan \phi$ would be achieved before the shear zone structure reduced the strength to $\sin \phi$.

In either of the models outlined above, it would also be advantageous to reconcile results from both intact and granular material, as suggested by LOCKNER and BYERLEE (1993). The slightly greater strength of overconsolidated gouge suggests that it may represent a state mid-way between intact rock and normally-consolidated gouge.

Although a single preferred model is not proposed here, it is clear that geometrically simple and carefully-controlled laboratory experiments are exposing inconsistencies in mechanical behavior. The structural complexity encountered on the geological scale is unlikely to simplify matters. It therefore seems imperative to establish a self-consistent description based on laboratory experiments before complete confidence can be attached to interpretation of field measurements of stress and strain.

4.2 The Stability of Fault Gouge

Most recent discussions of fault stability have emphasized velocity-weakening of friction as the basic mechanism reponsible for earthquake nucleation. The results presented here invite a revisiting of strain-weakening as an instability mechanism (e.g., RICE, 1979; STUART, 1979; JONES, 1980).

It must first be acknowledged that any strain-weakening model must address the question of strength recovery between earthquakes. For example, a recovery in the cohesion of fault rocks, due to healing of contacts across a fault plane broken during an earthquake, might return the fault to an unstable state. This effect is exemplified by the experimental results summarized in Figure 13 of CHESTER and LOGAN (1986), showing a gradation in mechanical behavior between intact rock, faulted rock and gouge from the Punchbowl Fault in Southern California. Intact samples fail with abrupt strain-weakening at small strains, but faulted samples reveal mild strain-weakening at larger strains. The gouge samples never reached failure. These results suggest that strain across the fault zone as a whole would be preferentially accommodated in the gouge layer, and would be stable. The recovery of some cohesion in the gouge, by a process of recementation, would be needed to produce unstable behavior.

Considering the results presented here, the potential for strain-weakening in fault gouge might alternatively be related to the porosity of the material, or the degree of overconsolidation. Normally consolidated samples (higher porosity) require large shear strains to reach failure and do not appear to strain-weaken significantly. Subject to the uncertainties in correcting the axial stress, the latter conclusion can be defended for both the fixed-end (no strain localisation) or free-end (strain localised to a fault) experiments. Overconsolidated samples (smaller porosity) require smaller shear strains to reach failure and have somewhat greater failure strength than normally consolidated samples. There is clear evidence of strain weakening in the experiments shown in Figure 5. Also, the fact that the overconsolidated samples appear to dilate back up towards the post-failure porosity of normally consolidated samples is consistent with strain-weakening.

The process of healing remains problematic. If overconsolidated gouge relaxes back towards a normally consolidated state after failure, it would then need to become overconsolidated again before instability could recur. The overconsolidation procedure used in these experiments was to substantially increase the level of effective stress without causing failure. In nature, the only conceivable way that the effective stress might be increased would be through a large decrease in pore fluid pressure.

More probably, the chemical action of pore fluid in the deeper, hotter parts of the seismogenic zone might promote overconsolidation through creep. This suggestion entails an extension of the purely mechanical concept of overconsolidation, but any mechanism of porosity reduction should have similar effects on the failure conditions. Also, a process of overconsolidation by creep would presumably result

in some recovery of cohesion. Intriguingly, the transition of the fault zone from a stable state to an unstable state would depend on time and the local conditions such as pressure, temperature and fluid chemistry.

This discussion suggests the following conceptual model of a fault zone containing a gouge layer. Shallower, cooler regions contain stable, normally consolidated gouge, while deeper, hotter regions contain gouge that becomes overconsolidated, cohesive and unstable with time. If the gouge layer were of roughly constant thickness, the rate of strain accumulation in the gouge layer would also be roughly constant. Earthquakes would nucleate in the deeper regions long before the shallow regions approached failure, because the strain at failure of overconsolidated gouge is relatively small. Assuming that the stress amplification associated with dynamic rupture carried faulting through into the shallow regions, coseismic relief of tectonic stress and strain would occur at all depths. Thus, the stress and apparent strength of the fault zone at shallow levels would remain small throughout the earthquake cycle.

A. Corrections to Axial Stress for Changes in Sample Cross Section

A.1 Isotropic Loading

The initial sample radius r_0, and length z_0 are measured at room pressure. The volume is calculated as $v_0 = \pi r_0^2 z_0$. The sample is then loaded isotropically, without contact from the axial piston, by increasing the confining pressure to $p_c = 160$ MPa (with $p_p = 10$ MPa). This loading causes a significant volumetric strain, typically around -0.15. Neither the axial or radial strain associated with this initial loading are measured (during axial loading, the axial shortening is measured from the displacement of the loading piston). In order to calculate the new sample dimensions, the assumption is made that the strain is isotropic, i.e.,

$$\epsilon_z = \epsilon_r = \tfrac{1}{3}\epsilon_v \tag{3}$$

where ϵ_z, ϵ_r and ϵ_v are the axial, radial and volumetric strains.

For the relatively large strains involved here, the components of strain are given by the following logarithmic forms:

$$\epsilon_z = \ln\left(\frac{z_1}{z_0}\right) \tag{4}$$

$$\epsilon_r = \ln\left(\frac{r_1}{r_0}\right) \tag{5}$$

$$\epsilon_v = \ln\left(\frac{v_1}{v_0}\right) \tag{6}$$

where z_1, r_1 and v_1 are the sample length, radius and volume after isotropic loading.

From equations (3)–(6), the length and cross-sectional area of the sample after isotropic loading are given by:

$$\frac{z_1}{z_0} = \left(\frac{v_1}{v_0}\right)^{1/3} \tag{7}$$

$$\frac{A_1}{A_0} = \left(\frac{r_1}{r_0}\right)^2 = \left(\frac{v_1}{v_0}\right)^{2/3} \tag{8}$$

where A_0 and A_1 are the cross-sectional areas of the sample before and after isotropic loading.

A.2 Axial Loading with Uniform Strain

In performing this correction the sample is assumed to retain a uniform right-cylindrical shape. The axial and volumetric strains are measured directly, and the radial strain can be calculated as follows:

$$2\epsilon_r = \epsilon_v - \epsilon_z. \tag{9}$$

Using equation (9) and logarithmic forms similar to equations (4), (5) and (6), the sample radius can be related to the observed sample length and volume. The following relation can then be derived, giving the cross-sectional area of the sample A relative to its state after isotropic loading:

$$\left(\frac{A}{A_1}\right) = \left(\frac{r}{r_1}\right)^2 = \frac{v}{v_1}\frac{z_1}{z} \tag{10}$$

where A, r, z, and v are the sample dimensions during axial loading.

The sample, of cross-sectional area A, is loaded axially by a piston of cross-sectional area A_0, and otherwise confined by a fluid at pressure p_c. The axial component of normal stress in the sample σ_z must be calculated from the measured force F exerted by the piston. Because the sample and piston have different radii, an equation for the axial force balance must account for the confining pressure acting on an annulus of material at the junction between the piston and sample.

$$F + (A - A_0)p_c = A\sigma_z. \tag{11}$$

Note that if $A < A_0$ the confining pressure acts on an exposed annulus of the piston and hence resists the force F, and *vice versa*. The uncorrected axial stress is by definition $\sigma_0 = F/A_0$, so the following correction formulation is obtained:

$$(\sigma_z - p_c) = \frac{A_0}{A}(\sigma_0 - p_c). \tag{12}$$

The area correction obtained from equations (8) and (10) is therefore applied to the differential stress $(\sigma_z - p_c)$, rather than the total axial stress σ_z.

A.3 Axial Loading with Fault Slip

When the strain in a sample localises to a single oblique fault, subsequent sample shortening is accommodated by fault slip. This slip reduces the effective cross-sectional area of the sample. By considering the area of overlap between two offset circles of equal radius, the following correction formula can be obtained for the cross-sectional area:

$$\frac{A_{\text{corr}}}{A} = \frac{\Theta - \sin \Theta}{\pi} \tag{13}$$

$$\Theta = \pi - 2 \sin^{-1}\left(\frac{\delta z}{2r} \tan \psi\right) \tag{14}$$

where A and A_{corr} are the original and corrected cross-sectional areas of the sample, δz is the amount of sample shortening due to fault slip, r is the sample radius and ψ is the angle between the fault plane and the axis of the sample. Θ is the angle subtended by the points of intersection of two overlapping circles, at the centers of the circles.

Acknowledgments

The authors would like to thank R. Summers for technical assistance. The manuscript was improved after helpful comments from the editors, and reviews from T. Shimamoto, B. Kilgore and one anonymous reviewer. DRS was supported by a Visiting Fellowship from the Southern California Earthquake Center and by an NERC Research Fellowship. Southern California Earthquake Center Publication Number 103.

REFERENCES

AMADEI, B., and ROBINSON, M. J., *Strength of rock in multiaxial loading conditions.* In *Proc. 27th U.S. Symp. on Rock Mechanics* (University of Alabama 1986) pp. 47–55.

BIEGEL, R. L., SAMMIS, C. G., and DIETERICH, J. H. (1989), *The Frictional Properties of a Simulated Gouge Having a Fractal Particle Distribution*, J. Struct. Geol. *11*, 827–846.

BYERLEE, J. D., and SAVAGE, J. C. (1993), *Coulomb Plasticity within the Fault Zone*, Geophys. Res. Lett. *19*, 2341–2344.

BYERLEE, J. D. (1978), *Friction of Rocks*, Pure Appl. Geophys. *116*, 615–626.

CHESTER, F. M., and LOGAN, J. M. (1987), *Composite Planar Fabric of Gouge from the Punchbowl Fault, California*, J. Struct. Geol. *9*, 621–634.

CHESTER, F. M., and LOGAN, J. M. (1986), *Implications for Mechanical Properties of Brittle Faults from Observations of the Punchbowl Fault Zone, California*, Pure Appl. Geophys. *124*, 79–106.

FREDRICH, J. T., and EVANS, B., *Strength recovery along simulated faults by solution transfer processes.* In *33rd U.S. Rock Mechanics Symposium* (eds. Tillerson, J. R., and Wawersik, W. R.) (Balkema, A. A., Rotterdam 1969) pp. 121–130.

GREEN, G. E., and BISHOP, A. W. (1969), *A Note on the Drained Strength of Sand under Generalized Strain Conditions*, Geotechnique *19*, 144–149.

HANSEN, B., *Shear box tests on sand.* In *Proc. 5th Int. Conf. on Soil Mech. and Found. Eng.* (ed. Dunod, Paris 1969) pp. 127–131.

HOBBS, B. E., ORD, A., and MARONE, C., *Dynamic behavior of rock joints.* In *Proc. Int. Symp. on Rock Joints* (eds. Barton, N. R., and Stephansson, O.) (Loen, Norway 1990) pp. 435–445.

JONES, L. M. (1981), *Field and Laboratory Studies of the Mechanics of Faulting*, Ph.D. Thesis, Massachusetts Institute of Technology, 106 pp.

JONES, L. M. (1980), *Cyclic Loading of Simulated Gouge to Large Strains*, J. Geophys. Res. *85*, 1826–1832.

LOCKNER, D. A., and BYERLEE, J. D. (1993), *How Geometric Constraints Contribute to the Weakness of Mature Faults*, Nature *363*, 250–252.

MANDL, G., *Mechanics of Tectonic Faulting* (Elsevier, Amsterdam 1988) 407 pp.

MANDL, G., DE JONG, L. N. J., and MALTHA, A. (1977), *Shear Zones in Granular Material*, Rock Mechanics *9*, 95–144.

MARONE, C., and KILGORE, B. (1993), *Scaling of the Critical Slip Distance for Seismic Faulting with Shear Strain in Fault Zones*, Nature *362*, 618–621.

MARONE, C., HOBBS, B. E., and ORD, A. (1992), *Coulomb Constitutive Laws for Friction: Contrasts in Frictional Behavior for Distributed and Localized Shear*, Pure Appl. Geophys. *139*, 195–214.

MARONE, C., and SCHOLZ, C. H. (1989), *Particle-size Distribution and Microstructures within Simulated Fault Gouge*, J. Struct. Geol. *11*, 799–814.

MOGI, K. (1967), *Effect of Intermediate Principal Stress on Rock Failure*, J. Geophys. Res. *72*, 5117–5131.

OAKESHOTT, G. B. (1958), *Geology and Mineral Deposits of San Fernando Quadrangle, Los Angeles County, California*, Calif. Div. Mines Bull. *172*, 147 pp.

RICE, J. R. (1979), *Theory of Precursory Processes in the Inception of Earthquake Rupture*, Gerlands Beitr. Geophysik *88*, 91–127.

RICE, J. R., *Fault stress states, pore pressure distributions, and the weakness of the San Andreas Fault.* In *Fault Mechanics and Transport Properties of Rocks* (eds. Evans, B., and Wong, T.-F.) (Academic Press, 1992) pp. 475–503.

SAMMIS, C. G., KING, G. C. P., and BIEGEL, R. L. (1987), *The Kinematics of Gouge Deformation*, Pure Appl. Geophys. *125*, 777–812.

SAMMIS, C. G., and BIEGEL, R. L. (1989), *Fractals, Fault-gouge, and Friction*, Pure Appl. Geophys. *131*, 255–271.

SCOTT, D. R., MARONE, C., and SAMMIS, C. G. (1994), *The Apparent Friction of Granular Fault Gouge in Sheared Layers*, J. Geophys. Res., in press.

STUART, W. D. (1979), *Strain Softening Prior to Two-dimensional Strike Slip Earthquakes*, J. Geophys. Res. *84*, 1063–1070.

TAKAHASHI, M., and KOIDE, H, *Effect of the intermediate principal stress on strength and deformation behavior of sedimentary rocks at depth shallower than 2000 m.* In *Rock at Great Depth* (eds. Maury and Fourmaintraux) (Balkema, Rotterdam 1992) pp. 19–26.

YAMAMURO, J. A., and LADE, P. V. (1993), *Instability and Behavior of Granular Materials at High Pressures*, Report No. UCLA-ENG-93-26, Civil Engineering Department, University of California, Los Angeles.

ZOBACK, M. D., and BYERLEE, J. D. (1976a), *A Note on the Deformational Behavior and Permeability of Crushed Granite*, Int. J. Rock Mech. Min. Sci. and Geomech. Abstr. *13*, 291–294.

ZOBACK, M. D., and BYERLEE, J. D. (1976b), *Effect of High-pressure Deformation on the Permeability of Ottawa Sand*, AAPG Bull. *60*, 1531–1542.

(Received October 8, 1993, revised January 10, 1994, accepted January 29, 1994)